

Electronic structure and magnetism of Mn-doped GaN

B. Sanyal, O. Bengone, and S. Mirbt

Department of Physics, Uppsala University, Uppsala, Sweden

(Received 23 May 2003; revised manuscript received 12 August 2003; published 21 November 2003)

Mn-doped semiconductors are extremely interesting systems due to their novel magnetic properties suitable for the spintronics applications. It has been shown recently by both theory and experiment that Mn-doped GaN systems have a very high Curie temperature compared to that of Mn-doped GaAs systems. To understand the electronic and magnetic properties, we have studied Mn-doped GaN system in detail by a first-principles plane-wave method. We show here the effect of varying Mn concentration on the electronic and magnetic properties. In agreement with previous studies, d states of Mn form an impurity band completely separated from the valence-band states of the host GaN for dilute Mn concentration. This is in contrast to the Mn-doped GaAs system where Mn d states in the gap lie very close to the valence-band edge and hybridize strongly with the delocalized valence-band states. To study the effects of electron correlation, LSDA+ U calculations have been performed. Calculated exchange interaction in (Mn,Ga)N is short ranged contrary to that in (Mn,Ga)As where the strength of the ferromagnetic coupling between Mn spins is not decreased substantially for large Mn-Mn separation. Also, the exchange interactions are anisotropic in different crystallographic directions due to the presence or absence of connectivity between Mn atoms through As bonds.

DOI: 10.1103/PhysRevB.68.205210

PACS number(s): 75.50.Pp, 71.70.Gm

I. INTRODUCTION

Diluted magnetic semiconductors (DMS) are considered to be potential candidates for present and future technological applications in semiconductor spintronics.¹ During the last decade, there have been numerous experimental and theoretical studies of II-VI, III-V, and IV-VI DMS. Among the III-V DMS, Mn-doped GaAs system has been studied rigorously for the last few years. This system shows a Curie temperature (T_C) of 110 K for a Mn-doping concentration of 10%. Despite several attempts, T_C could not be raised beyond 175 K. Recently, there have been reports of some room-temperature DMS. They include Mn-doped GaP,² Mn-doped chalcopyrite CdGeP₂,³ Mn-doped GaN,^{4,5} etc. The origin of ferromagnetism in these compounds is still under debate.⁶

Dietl *et al.*⁷ predicted theoretically a high Curie temperature (~ 400 K) for Mn-doped GaN (5% Mn). Their theory was based on a mean-field model of hole mediated ferromagnetism. As the Curie temperature for a Mn-doped GaAs system is comparatively lower, the theoretical prediction for a higher T_C drew much attention. Sasaki *et al.*⁴ grew wurtzite Mn-doped GaN films by the molecular-beam epitaxy method. Magnetic measurements showed a very high Curie temperature of about 940 K. They ruled out the possibility of phase segregation of some ferromagnetic compounds, e.g., MnGa and Mn₄N which also have high Curie temperatures. Room-temperature ferromagnetism in Mn-doped GaN was also observed by Reed *et al.*⁵ Deep level optical spectroscopy measurements⁸ show that Mn forms a deep acceptor level at 1.42 eV above the valence-band maximum for GaN doped with small concentration of Mn. It is to be noted that Mn forms an acceptor level at 0.11 eV above the valence-band maximum in the case of Mn-doped GaAs. So, the overlap of the Mn d -states with the valence-band is rather strong in Mn-doped GaAs compared to Mn-doped GaN.

Recently, there have been a few first-principles electronic

structure calculations of Mn-doped GaN systems. Fong *et al.*⁹ performed electronic structure calculations of Fe- and Mn-doped GaN using the tight-binding linearized muffin-tin orbital (TB-LMTO) method. Sato and Katayama-Yoshida¹⁰ performed Korringa-Kohn-Rostoker coherent potential approximation calculations to study the relative stabilities of ferromagnetic and spin-glass phases. They showed that for a low concentration of Mn, ferromagnetism is favored whereas for the high concentration, the spin-glass phase is stable. The disordered local-moment model was assumed to describe the spin-glass phase. They explained the origin of ferromagnetism in these systems by a competition between double-exchange and superexchange interactions. Kulatov *et al.*¹¹ studied electronic, magnetic, and optical properties of zinc blende (Mn,Ga)N for different concentrations of Mn by the TB-LMTO method in a supercell approach. Anomalous exchange interactions in III-V DMS were found from calculations by Schilfgaard and Mryasov.¹² They predicted aggregation of magnetic nanoclusters inside the III-V host. Kronik *et al.*¹³ considered (Mn,Ga)N in wurtzite structure and performed electronic structure calculations using a plane-wave pseudopotential method. In Ref. 14, the different origins of ferromagnetism in (Mn,Ga)As and (Mn,Ga)N systems were discussed. The authors pointed out from self-interaction corrected (SIC) pseudopotential calculations that (Mn,Ga)N is characterized by localized Mn $3d$ states with a strong self-interaction. In (Mn,Ga)As, d states are weakly correlated and are rather delocalized being strongly hybridized with As p states. In this paper, we attempt to understand the electronic structure and magnetic interactions in Mn-doped GaN and GaAs systems. The motivation of this paper is twofold: (a) to investigate electronic structure and magnetism of Mn-doped GaN system in detail and (b) to have a comparison with Mn-doped GaAs system. The paper is organized as follows: In the following section, we describe the computational details. Section. III A describes the electronic structure and magnetism of the (Mn,Ga)N with varying Mn concentration

in the local spin-density approximation (LSDA). Then we present results from LSDA+ U calculations. Finally, we show a comparison of exchange interactions in (Mn,Ga)N and (Mn,Ga)As systems.

II. COMPUTATIONAL DETAILS

GaN can be grown both in the zinc blende and wurtzite structures. But, usually, Mn is doped in a wurtzite GaN host.⁴ In our calculations, we have considered the wurtzite structure. Also, for a comparison, we show calculations for the zinc blende structure. Experimental lattice parameters such as $a=3.189$ Å and $c=5.185$ Å with a c/a ratio of 1.626 were taken for the calculations in the wurtzite structure. Results from the atomic relaxations revealed that the nearest-neighbor bond lengths between Mn and N change only by 3% compared to that of the bulk GaN. This is in agreement with the results of Kronik *et al.*¹³ In general, Mn doping in substitutional site results in a small relaxation¹⁵ of the nearest-neighbor anions around it.

Calculations have been performed by an *ab initio* plane-wave code (VASP),¹⁶ Vanderbilt type¹⁷ ultrasoft pseudopotentials were used for the LSDA calculations. LSDA+ U calculations were done in the projector augmented wave¹⁸ method as implemented by Bengone *et al.*¹⁹ Ga $3d$ orbitals were included in the basis set of the Ga pseudopotential. A kinetic-energy cutoff of 350 eV was used for the plane waves included in the basis set. Ceperley and Alder²⁰ exchange-correlation functional parametrized by Perdew and Zunger²¹ was considered within LSDA. We have also checked that the results obtained within GGA (generalized gradient approximation²²) are similar. A $8 \times 8 \times 6$ k -points grid was used in the Monkhorst-Pack scheme²³ for small supercells. For the largest supercell considered, a $2 \times 2 \times 1$ grid was used. Local properties such as local density of states and local magnetic moments were calculated by projecting the wave functions onto spherical harmonics.²⁴ The radii chosen for the projection were 1.31, 1.21, and 0.74 Å for Mn, Ga, and N, respectively.

We have modeled the system using different supercell sizes to simulate different Mn concentrations. For wurtzite structure, supercells having 4, 8, 16, 32, 72, and 108 atoms were used to model a composition $\text{Mn}_x\text{Ga}_{1-x}\text{N}$ for $x=0.5$, 0.25, 0.125, 0.0625, 0.028, and 0.018, respectively. For zinc blende structure, we used a 64-atom cell to simulate a Mn concentration of $x=0.03125$. It has been found experimentally that Mn occupies the Ga site.²⁵ Therefore, in our calculational unit cell, a Ga atom was substituted by a Mn atom.

III. RESULTS

A. Calculations within LSDA

In a III-V semiconductor, a cation vacancy creates three holes in the valence band leaving anion dangling bonds. When Mn occupies the cation site, it donates three electrons to fulfill the bonding. Mn is left with four unpaired d electrons which give rise to $4 \mu_B/\text{Mn}$ atom. In a realistic situation, there can be compensating donors, e.g., As antisites and interstitial Mn atoms,²⁶ present in the system to increase or

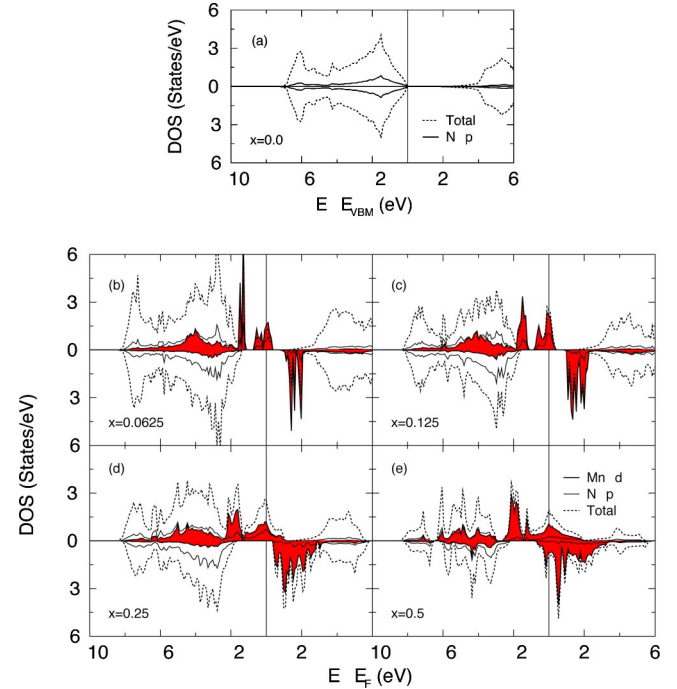


FIG. 1. Spin resolved density of states of $(\text{Mn}_x\text{Ga}_{1-x})\text{N}$ in the wurtzite structure. Data are shown for (a) pure GaN, (b) 6.25% Mn in GaN, (c) 12.5% Mn, (d) 25% Mn, and (e) 50% Mn. In (a), total DOS/cell as well as the p DOS of N have been shown whereas in (b)–(e), d DOS of Mn (in shade), p DOS of N, and total DOS have been plotted. Energies are plotted with reference to valence-band maximum (VBM) of GaN in (a) and Fermi energies E_F in (b)–(e).

decrease the magnetic moments. But as we are dealing with ideal uncompensated systems, we always obtain a magnetic moment of $4 \mu_B/\text{Mn}$ atom for substitutional Mn.

In Figs. 1(a)–1(e), we show the density of states (DOS) for various concentrations x of Mn in $\text{Mn}_x\text{Ga}_{1-x}\text{N}$ in the wurtzite structure. In Fig. 1(a), the DOS of the undoped GaN is presented. The large band gap is evident from the figure. The calculated direct band gap at the Γ point is 1.9 eV which is underestimated compared to the experimental band gap of ~ 3.4 eV. This well-known underestimation is inherent in the formulation of density-functional theory and is well documented in existing literature. From Fig. 1(b) to 1(e), we show the DOS's with increasing x . The Mn impurity d peak in the band gap is away from the valence band for small x . As the concentration increases, this peak is broadened due to the overlap of Mn d wave functions and the gap between the impurity peak and the valence-band edge vanishes. The total DOS/cell gradually regains the shape of the DOS of undoped system as x is reduced. However, up to $x=0.25$, the Fermi level cuts only the spin-up DOS's. As there is no state at Fermi level for the spin-down channel, we obtain a half-metallic solution giving rise to an integer magnetic moment of $4 \mu_B/\text{Mn}$ atom. For $x=0.5$ shown in Fig. 1(e), the system behaves like a ferromagnetic metal with a reduced magnetic moment. One noticeable difference between Mn-doped GaAs and Mn-doped GaN systems is the position of Mn impurity band in the gap. In (Mn,Ga)As, Mn impurity band almost merges with the top of the valence band (≈ 0.1 eV

TABLE I. Projected charges and magnetic moments (in μ_B). Mn- d^Q indicates charge in the sphere around Mn for d electrons. Mn $_{mom}$ and N $_{mom}$ indicate projected magnetic moments inside Mn and N spheres, respectively.

x in Mn $_x$ Ga $_{1-x}$ N	Mn- d^Q	Mn $_{mom}$	$\frac{1}{4}\sum_{nn} N_{mom}$
0.018	5.04	3.40	0.016
0.028	5.04	3.41	0.016
0.0625	5.05	3.43	0.01
0.125	5.05	3.42	0.015
0.25	5.04	3.47	0.02
0.50	5.09	2.61	-0.02

above the valence-band edge) whereas in (Mn,Ga)N, the Mn impurity band is separated from the valence band by 0.56 eV. The width of this impurity band is 0.94 eV. As the spin-polarized Mn impurity band is distinctly in the gap, the valence band is less spin polarized in (Mn,Ga)N compared to (Mn,Ga)As. Spin polarization ($\epsilon_{VBM/CBM}^\uparrow - \epsilon_{VBM/CBM}^\downarrow$) of the valence and conduction bands at the Γ point is 0.05 eV and -0.42 eV, respectively, for (Mn $_{0.0625}$ Ga $_{0.9375}$)N. ϵ is the eigenvalue and VBM and CBM represent valence-band maximum and conduction band minimum, respectively. Our LSDA calculations are in excellent agreement with previous studies. Kronik *et al.*¹³ also found 100% spin-polarized impurity band in the host band gap with the Fermi level lying in the impurity band. Band-structure plots done by Filippetti *et al.*¹⁴ also confirmed this.

In Table I, we present the local charges and magnetic moments of Mn and N atoms for different concentrations of Mn. Charges and magnetic moments of Mn remain almost the same with the concentration variation of Mn. The insensitivity of magnetic moment with concentration is a signature of localized d states of Mn. The total moment/cell is always $4.0 \mu_B$ which is the signature of a half-metallic solution. The only exception is the case of $x=0.5$, where the total moment/cell is $2.77 \mu_B$. The exchange splitting of Mn d states is less in this case allowing both spin-up and spin-down d states to cross the Fermi level. The averaged induced moments on nearest-neighbor N atoms are also tabulated. In most of the cases, the moments are parallel to Mn moments which is not the case for a Mn-doped GaAs system where nearest-neighbor As moments are antiferromagnetically coupled to the Mn magnetic moment.

As GaN can be grown in both zinc blende and wurtzite structures, we have also done calculations for a 6.5% Mn-doped GaN system in zinc blende structure. In Fig. 2, DOS's for both structures are shown. DOS for a zinc blende structure is similar to that calculated by Kulatov *et al.*¹¹ Also the magnetic moment on Mn atom ($3.4 \mu_B$) agrees very well. There is no striking difference in the broad features of the DOS's for the two structures. In the zinc blende structure, the peak at the Fermi level is sharper and the nature of these states are different (t_2 compared to e states for the wurtzite structure). See Fig. 5 and related discussions. For both the structures, the Mn impurity peak in the energy gap of the host is separated from the valence band of the host.

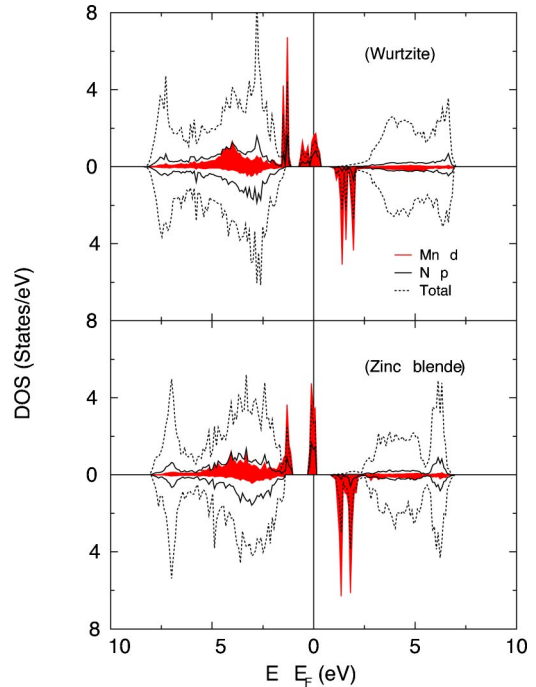


FIG. 2. Spin resolved density of states of (Mn,Ga)N for (top) wurtzite and (b) zinc blende structures. Here, the Mn concentration is 6.25%.

B. LSDA+ U calculations

It is a matter of debate whether the itinerant band model or the localized atomic model is appropriate for the description of Mn-doped semiconductors. Density-functional calculations^{15,27-29} based on LSDA or GGA provide the basis of itinerant picture whereas others models are based on a localized atomic picture.⁷ A recent photoemission experiment³⁰ on Mn-doped GaAs system revealed the main Mn d peak to be situated 3.4 eV below the Fermi level. A previous photoemission experiment³¹ reported the peak to be 4.4 eV below the Fermi level. Also, the importance of electron-correlation effects in these systems was highlighted. Park *et al.*³² argued from LSDA+ U calculations that correlation corrections are important to have a better agreement with photoemission spectra. On the other hand, all density-functional calculations based on LSDA show a peak around 2.6–2.9 eV below the Fermi level.^{15,27} So it can be argued that the completely localized picture or the completely itinerant picture cannot solely describe these systems satisfactorily.

We have done LSDA+ U calculations to investigate the effect of electron correlations. First, these calculations do not exist in literature and second, it is interesting to compare this simple technique with more rigorous SIC calculations. In Figs. 3(a)–3(d), we show the DOS's obtained from LSDA and LSDA+ U calculations for 6.25% Mn. As the value of U for Mn d states is not obtained self-consistently from first-principles calculations, we varied U from 4 eV to 7 eV treating it as a parameter. In all cases, the exchange parameter J was considered to be 1.0 eV. Increasing U results in a slow shift of the spin-up impurity band towards the valence band. The small peak around 1.5 eV below the Fermi level E_F is

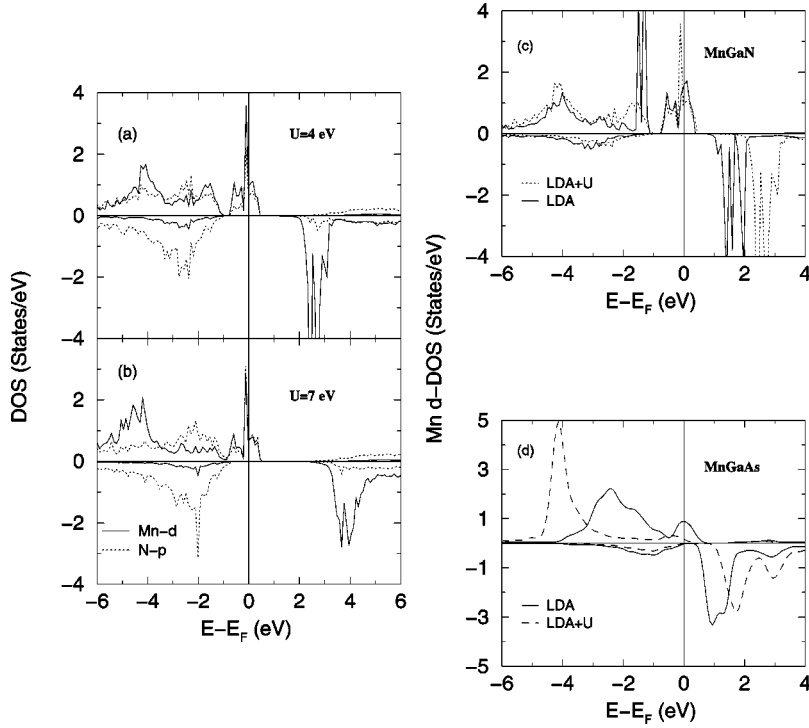


FIG. 3. (a) and (b) Spin resolved Mn d and N p DOS's from the LSDA+ U calculations for different values of U for (Mn,Ga)N system in the wurtzite structure, (c) Mn d -DOS from both LSDA and LSDA+ U calculations for (Mn,Ga)N in the wurtzite structure, and (d) same as (c), but for (Mn,Ga)As in the zinc blende structure. For all plots, Mn concentration is 6.25%.

diminished gradually in magnitude whereas the peak around -4.5 eV below E_F increases in magnitude. Even for $U = 10$ eV (not shown here), the localized peak remains pinned close to E_F and is *not* merged with the delocalized valence-band states. The spin-down DOS shifts almost rigidly away from the Fermi level towards higher energy with increasing U . Local charges and magnetic moments of Mn and nearest-neighbor N atoms are listed in Table II. Magnetic moment of Mn increases with U due to increase in localization of d states. The induced moments of N atoms also increase. In Fig. 3(c), a comparison between LSDA and LSDA+ U calculations is shown. The redistribution of weights of Mn d peaks with the inclusion of U is visible. In LSDA+ U result, the sharp peak is very close to the Fermi level in the impurity band whereas it is in the valence band in the LSDA calculation. This peak is of e character and does not take part in the bonding with the neighboring N atoms. These results are in agreement with the more sophisticated SIC calculations reported by Filippetti *et al.*¹⁴ They also found a flat band with d_{z^2} character at E_F . The nature of the states close to E_F from our calculation is shown later in Fig. 5. To our knowledge, the valence-band photoemission spectra of (Mn,Ga)N is not available in the literature. So, the extent of validity of LSDA approach cannot be tested. Our LSDA+ U findings can be compared with future angle-resolved photoemission experi-

TABLE II. Projected charges and magnetic moments (in μ_B) calculated within LSDA+ U . The notations are same as in Table I.

	$U=4.0$ eV	$U=5.0$ eV	$U=6.0$ eV	$U=7.0$ eV
Mn- d^Q	5.01	5.00	4.99	4.98
Mn $_{mom}$	3.72	3.83	3.93	4.02
N $_{mom}^{mn}$	-0.02	-0.04	-0.05	-0.06

ments on (Mn,Ga)N to verify the existence of the localized peak close to E_F . A comparative study with Mn-doped GaAs is shown in Fig. 3(d). The main broad Mn d peak around 2.8 eV below the Fermi level in a LSDA calculation is shifted 4 eV below the Fermi level with a smaller bandwidth. The DOS at the Fermi level is also decreased compared to that of an LSDA calculation. In both LSDA and LSDA+ U calculations, the hybridization between Mn d and As p states are seen. So the holes in the valence band have hybridized p - d character. In the previous LSDA studies,^{13,14} a similar discussion on the nature of hybridization was also made.

In Fig. 4, we show the integrated magnetization density around various atoms in the unit cell as a function of the radius of integration. It has been calculated as

$$M(R) = \int_0^R [\rho^\uparrow(r) - \rho^\downarrow(r)] dr,$$

where $\rho^\uparrow(r)$ and $\rho^\downarrow(r)$ are the spin-up and spin-down charge densities, respectively, and M is the magnetic moment obtained for a radius R . For (Mn,Ga)N and (Mn,Ga)As in the zinc blende structure, the magnetic moment reaches the value $4 \mu_B$ at a distance of 5 \AA far from the Mn center. But, in the wurtzite structure of (Mn,Ga)N, this value is reached at a smaller distance. This again shows a more localized character of Mn d states in wurtzite GaN. The integration around nearest-neighbor anions reveals that N has a positive contribution in (Mn,Ga)N whereas As has a negative contribution.

In Fig. 5, we show the character of the states within an energy interval close to the Fermi level. The states close to E_F in the electronic structure are important in characterizing the origin of ferromagnetism. The projection of the wave function onto spherical harmonics around each atom has

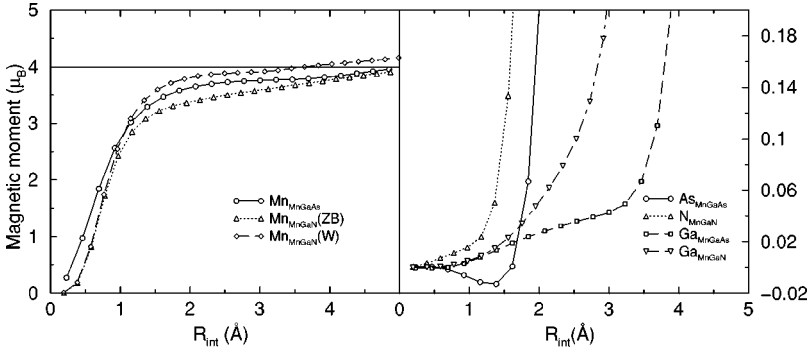


FIG. 4. Magnetic moment vs radius of integration around specific atoms. In (a) integrated magnetization density around Mn spheres and in (b) the same around nearest-neighbor anions and next-nearest-neighbor Ga atoms are shown. See text for details. The horizontal line in the left figure indicates a magnetic moment of $4 \mu_B$. ZB and W represent zinc blende and wurtzite structures, respectively.

been calculated as mentioned in Ref. 24. In the figure, χ is defined as $\chi_{lm}^{N,\sigma} = \sum_{nk} |Y_{lm}^{N,\sigma}(\phi_{nk}^\sigma)|^2$, where σ and N are the spin and atom indices, respectively, and n is the index for the bands within the specified energy interval. It is clear from the figure that for (Mn,Ga)N in the wurtzite structure (left panel), the d_{z^2} component of Mn e orbital and the p_z component of nearest-neighbor N p orbital are the dominant states close to E_F . On the other hand, Mn t_2 and nearest-neighbor As p states hybridize strongly in (Mn,Ga)As. This is also true for (Mn,Ga)N in the zinc blende structure. Symmetry of the crystal structure and the splitting of d states under the corresponding crystal fields determine the position of t_2 and e states. For the rest of the atoms in the unit cell, states having s and p character are the dominant.

IV. INTERATOMIC EXCHANGE INTERACTIONS

To determine the interatomic exchange interactions, we followed a simple model. In the unit cell, two Mn atoms

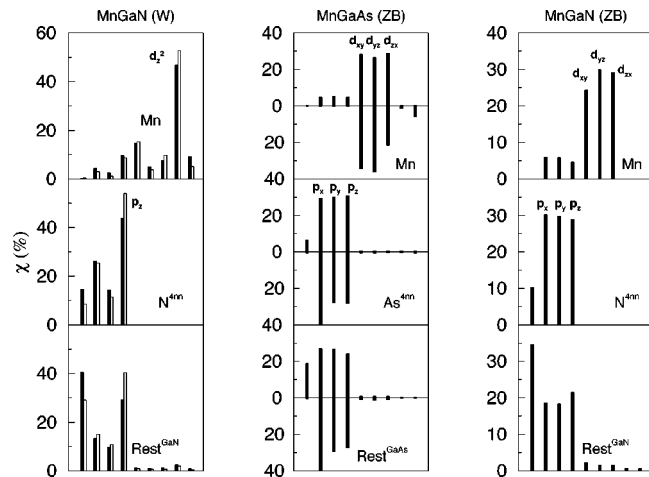


FIG. 5. Character of states within an energy interval from E_F to $E_F - 0.5$ eV for (left) (Mn,Ga)N in the wurtzite structure, (middle) (Mn,Ga)As in the zinc blende structure, and (right) (Mn,Ga)N in the zinc blende structure having 6.25% Mn in all cases. In x axis, the plotted states are in the order s , p_x , p_y , p_z , d_{xy} , d_{yz} , d_{zx} , d_{z^2} , $d_{x^2-y^2}$ from left. See text for details. For the middle panel, both spin-up and spin-down contributions are shown whereas for the left and right panels, there is no state in the spin-down channel. In the left column, the empty bars represent LSDA+ U values. For each panel, data are shown for Mn (top), four nearest-neighbor (nn) anions (middle), and the collective contributions from all other atoms (bottom) in the unit cell.

were placed in various positions. For each Mn-Mn separation, ferromagnetic (FM) and antiferromagnetic (AFM) alignments of Mn spins were considered. The total-energy difference ΔE ($\Delta E = E_{tot}^{AFM} - E_{tot}^{FM}$) between these two alignments is a measure of interatomic exchange interaction. In Fig. 6, we plot ΔE as a function of Mn-Mn separation d for both Mn-doped GaAs and Mn-doped GaN systems. For Mn-doped GaN, both zinc blende and wurtzite structures were considered for these calculations with two Mn atoms in unit cells having 64 atoms and 72 atoms, respectively. For Mn-doped GaAs, a 64-atom unit cell was chosen. Ferromagnetic interaction between Mn spins is favored for all the cases considered here. In (Mn,Ga)N, the first nearest-neighbor (nn) exchange interaction is the strongest. The value of ΔE is increased a little bit compared to the same for (Mn,Ga)As. So, for a defect-free calculation, there is no indication that (Mn,Ga)N should have a much higher T_C than (Mn,Ga)As. It suggests that the formation of other phases during the growth is responsible for very high T_C observed in certain experiments. It is also seen from the figure that ΔE decreases sharply with d for Mn-doped GaN systems. It shows that ferromagnetic exchange interaction in (Mn,Ga)N is short ranged. This indicates that the formation of Mn clusters

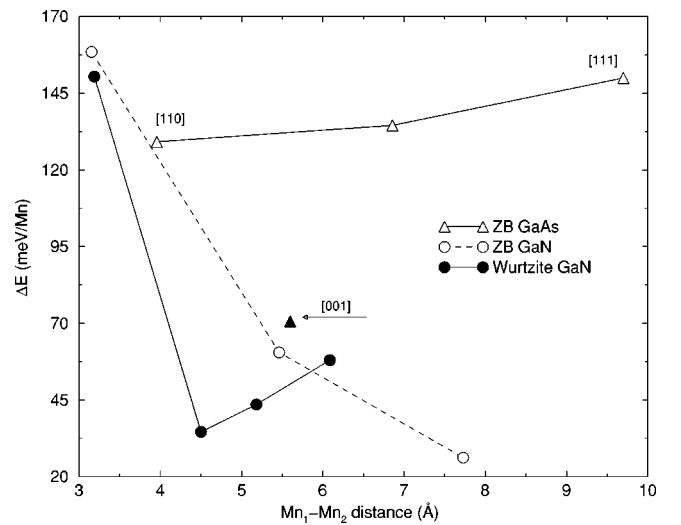


FIG. 6. Total-energy difference ΔE between ferromagnetic and antiferromagnetic configurations vs Mn-Mn distance in the unit cell. Data for zinc blende (ZB) GaN, ZB GaAs, and wurtzite (W) GaN are shown. The filled triangle represents ΔE for [001] direction in ZB GaAs.

within a short radial distance might lead to high values of T_C . For Mn-doped GaAs, the exchange interaction is long ranged and does not decrease rapidly. The proper range of ferromagnetic interactions can be studied with a bigger supercell. In summary, the results for exchange interactions indicate that the ferromagnetic interaction between Mn spins in (Mn,Ga)As is mediated by delocalized valence-band holes whereas the origin of ferromagnetism in (Mn,Ga)N may result from a double-exchange mechanism¹⁰ involving the hopping of Mn d electrons. The other probable mechanism can be the formation of Zhang-Rice magnetic polaron.³³

Another interesting observation is the anisotropy of the exchange interactions in different crystallographic directions. In (Mn,Ga)As, ferromagnetic coupling is stronger either in the bonding direction, e.g., [111] or in a direction where the two Mn spins are connected by As bonds, e.g., in [110] direction. The coupling decreases for the [001] direction where there is no As atom in between (shown as a filled triangle in Fig. 6). The strong ferromagnetic interactions in [110] or [111] directions result from strong p - d hybridization between Mn d and As p states. As the interaction is mediated by the delocalized states, they are sufficiently long ranged. In [001] direction, the exchange interaction between the Mn spins cannot be mediated by the p - d hybridization. So, the value of ΔE is decreased compared to the other cases. In (Mn,Ga)N, the exchange interaction is not mediated by the delocalized valence-band states and the ferromagnetic interactions decrease sharply with the Mn-Mn separation. So, the anisotropy in the exchange interactions is not significantly observed. We can conclude that, in general, this anisotropy should be present for all Mn-doped semiconductors where ferromagnetic long-range interaction is mediated by delocalized valence-band states. We also studied the exchange interactions in (Mn,Ga)N within the LSDA+ U scheme in a similar way described above. $U=4$ eV and $U=7$ eV were considered for the calculations. We found that ΔE for nearest-neighbor Mn-Mn distance increases from 170 meV/Mn to 240 meV/Mn while going from $U=4$ eV to U

$=7$ eV. Ferromagnetic interactions between Mn spins become stronger as the localization of the Mn d states is increased.

V. CONCLUSION

We have studied the electronic structure and magnetism of Mn-doped GaN systems for a wide concentration range of Mn. The deep acceptor level of Mn lies distinctly in the gap of GaN, separated from the valence band of host GaN. This is in contrast to the case of (Mn,Ga)As where the Mn forms shallow acceptor level close to the valence band of GaAs. Ferromagnetic interactions are short ranged in (Mn,Ga)N systems whereas they have delocalized itinerant character for (Mn,Ga)As. Also, in (Mn,Ga)As, exchange interactions are significantly anisotropic in different crystallographic directions. This has been explained in terms of anisotropic p - d hybridization. The results presented here are for ideal systems having no contribution from the native defects formed during the nonequilibrium growth. To have a more realistic picture, one should take into account these effects. Also, Mn can occupy interstitial positions in the lattice and the spin interactions can become quite complicated. We are presently calculating the formation energies of the defects and subsequently the magnetic interactions in presence of them. Results will be reported in future papers.

ACKNOWLEDGMENTS

We are grateful to the Swedish Foundation for Strategic Research (SSF), the Swedish Natural Science Research Council (NFR), and the Göran Gustafsson Foundation for financial support. We thank J. Hafner and G. Kresse for giving us the possibility to use VASP. B.S. is grateful to Dr. Lars Nordström and Professor Olle Eriksson for valuable suggestions. Also, we acknowledge computational support from National Supercomputer Center (NSC) at Linköping, Sweden.

¹*Semiconductor Spintronics and Quantum Computation*, edited by D. D. Awschalom, D. Loss, and N. Samarth (Springer, Berlin, 2002).

²N. Theodoropoulou, A.F. Hebard, M.E. Overberg, C.R. Abernathy, S.J. Pearton, S.N.G. Chu, and R.G. Wilson, *Phys. Rev. Lett.* **89**, 107203 (2002).

³G.A. Medvedkin, T. Ishibashi, T. Nishi, K. Hayata, Y. Hasegawa, and K. Sato, *Jpn. J. Appl. Phys., Part 2* **39**, L949 (2000).

⁴T. Sasaki, S. Sonada, Y. Yamamoto, K. Suga, S. Shimizu, K. Kindo, and H. Hori, *Jpn. J. Appl. Phys., Part 1* **91**, 7911 (2002).

⁵M.L. Reed, N.A. El-Masry, H.H. Stadelmaier, M.K. Ritums, M.J. Reed, C.A. Parker, J.C. Roberts, and S.M. Bedair, *Appl. Phys. Lett.* **79**, 3473 (2001).

⁶P. Kacman, *Semicond. Sci. Technol.* **16**, R25 (2001).

⁷T. Dietl, H. Ohno, and F. Matsukara, *Phys. Rev. B* **63**, 195205 (2001).

⁸R.Y. Korotkov, J.M. Gregie, and B.W. Wessels, *Appl. Phys. Lett.*

80, 1731 (2002).

⁹C.Y. Fong, V.A. Gubanov, and C. Boekema, *J. Electron. Mater.* **29**, 1067 (2000).

¹⁰K. Sato and H. Katayama-Yoshida, *Semicond. Sci. Technol.* **17**, 367 (2002).

¹¹E. Kulatov, H. Nakayama, H. Mariette, H. Ohta, and Yu.A. Usenskii, *Phys. Rev. B* **66**, 045203 (2002).

¹²M.V. Schilfgaard and O.N. Myrasov, *Phys. Rev. B* **63**, 233205 (2001).

¹³L. Kronik, M. Jain, and R. Chelikowsky, *Phys. Rev. B* **66**, 041203 (2002).

¹⁴A. Filippetti, N.A. Spaldin, and S. Sanvito, *cond-mat/0302178* (unpublished); available at <http://xxx.lanl.gov>

¹⁵S. Mirbt, B. Sanyal, and P. Mohn, *J. Phys.: Condens. Matter* **14**, 3295 (2002).

¹⁶G. Kresse and J. Hafner, *Phys. Rev. B* **47**, RC558 (1993); G. Kresse and J. Furthmüller, *ibid.* **54**, 11 169 (1996).

- ¹⁷D. Vanderbilt, Phys. Rev. B **41**, 7892 (1990).
- ¹⁸P.E. Blöchl, Phys. Rev. B **50**, 17 953 (1994).
- ¹⁹O. Bengone, M. Alouani, P.E. Blöchl, and J. Hugel, Phys. Rev. B **62**, 16 392 (2000).
- ²⁰D.M. Ceperley and B.J. Alder, Phys. Rev. Lett. **45**, 566 (1980).
- ²¹J. Perdew and A. Zunger, Phys. Rev. B **23**, 5048 (1981).
- ²²J.P. Perdew and Y. Yang, Phys. Rev. B **45**, 13 244 (1992).
- ²³H.J. Monkhorst and J.D. Pack, Phys. Rev. B **13**, 5188 (1976).
- ²⁴A. Eichler, J. Hafner, J. Furthmüller, and G. Kresse, Surf. Sci. **346**, 300 (1996).
- ²⁵M. Sato, H. Tanida, K. Kato, T. Sasaki, Y. Yamamoto, S. Sonoda, S. Shimizu, and H. Hori, Jpn. J. Appl. Phys., Part 1 **41**, 4513 (2002).
- ²⁶L. Bergqvist, P.A. Korzhavyi, B. Sanyal, S. Mirbt, I.A. Abrikosov, L. Nordström, E.A. Smirnova, P. Mohn, P. Svedlindh, and O. Eriksson, Phys. Rev. B **67**, 205201 (2003).
- ²⁷S. Sanvito, G. Theurich, and N.A. Hill, J. Supercond. **15**, 85 (2002).
- ²⁸Y. Zhao, W.T. Geng, K.T. Park, and A.J. Freeman, Phys. Rev. B **64**, 035207 (2001).
- ²⁹W.J.M. de Jonge and H.J.M. Swagten, J. Magn. Magn. Mater. **100**, 322 (1991).
- ³⁰H. Asklund, L. Ilver, J. Kanski, J. Sadowski, and R. Mathieu, Phys. Rev. B **66**, 115319 (2002).
- ³¹J. Okabayashi, A. Kimura, T. Mizokawa, A. Fujimori, T. Hayashi, and M. Tanaka, Phys. Rev. B **59**, R2486 (1999).
- ³²J.H. Park, S.K. Kwon, and B.I. Min, Physica B **281-282**, 703 (2000).
- ³³T. Dietl, F. Matsukara, and H. Ohno, Phys. Rev. B **66**, 033203 (2002).